

Performance Evaluation of a Next-Generation SX-Aurora TSUBASA Vector Supercomputer

Keichi Takahashi¹[0000-0002-1607-5694], Soya Fujimoto², Satoru Nagase², Yoko Isobe²,
Yoichi Shimomura¹, Ryusuke Egawa³[0000-0001-8966-867X], and Hiroyuki
Takizawa¹[0000-0003-2858-3140]

¹ Tohoku University

{keichi, shimomura32, takizawa}@tohoku.ac.jp

² NEC Corporation

{s-fujimoto, s.nagase, y-isobe-pi}@nec.com

³ Tokyo Denki University

egawa@mail.dendai.ac.jp

Abstract. Data movement is a key bottleneck in terms of both performance and energy efficiency in modern HPC systems. The NEC SX-series supercomputers have a long history of accelerating memory-intensive HPC applications by providing sufficient memory bandwidth to applications. In this paper, we analyze the performance of a prototype SX-Aurora TSUBASA supercomputer equipped with the brand-new Vector Engine (VE30) processor. VE30 is the first major update to the Vector Engine processor series, and offers significantly improved memory access performance due to its renewed memory subsystem. Moreover, it introduces new instructions and incorporates architectural advancements tailored for accelerating memory-intensive applications. Using standard benchmarks, we demonstrate that VE30 considerably outperforms other processors in both performance and efficiency of memory-intensive applications. We also evaluate VE30 using applications including SPEChpc, and show that VE30 can run real-world applications with high performance. Finally, we discuss performance tuning techniques to obtain maximum performance from VE30.

Keywords: performance evaluation · SX-Aurora TSUBASA · memory-intensive applications · vector processor · vector supercomputer

1 Introduction

The *memory wall* is a longstanding challenge in HPC that refers to the continuously widening gap between arithmetic computing performance and memory performance in a computing system. Due to the memory wall problem, memory-intensive applications are bottlenecked by data movement and unable to fully utilize the arithmetic computing performance of a system. Not only does this hurt the performance of applications, but it also degrades energy efficiency. The HPC community has therefore been actively exploring novel architectures to tackle the memory wall, such as adopting high-bandwidth memory devices for off-chip memory [3, 21], implementing large amounts of on-chip

memory [13, 18], and reducing memory accesses by directly exchanging data between processing elements [8, 9].

However, these exotic architectures completely differ from general-purpose CPUs, and often require the programmer to become familiar with unconventional programming models. For example, the device could require multiple magnitudes larger degree of parallelism than a CPU, or data movement across the memory subsystem might require explicit management by the programmer. As a consequence, developing software for such emerging hardware is generally time-consuming and expensive. If a large body of users exists, the cost for developing optimized software for a specialized system could be amortized (*e.g.*, deep learning). However, it is often the case in HPC that a scientifically important software package is maintained by a handful of programmers and used by a small group of users. In such a case, the development cost becomes prohibitive.

NEC's SX-Aurora TSUBASA (SX-AT) supercomputer aims to achieve both world-class memory performance and high productivity by a unique combination of latest memory technology with the vector architecture. The vector architecture has a long history and recently regained interests from the community. This trend can be seen in the ARM Scalable Vector Extension [25] and upcoming RISC-V Vector Extension [17], both of which are heavily inspired by the vector architecture. Since most HPC applications exhibit high data-level parallelism that can be automatically exploited by a vectorizing compiler, conventional software targeted for general-purpose CPUs can run with minor modifications. To keep feeding data to the high-performance vector cores, High Bandwidth Memory (HBM) is tightly coupled with the processor. As a result, SX-AT offers massive memory performance to applications while ensuring programmer productivity.

NEC has recently been prototyping a brand-new vector processor named Vector Engine 3.0 (VE30) for SX-AT. VE30 takes a big leap from the previous Vector Engine series, and brings a number of architectural advancements beyond peak compute and memory performance increase. Specifically, VE30 introduces bypassable per-core private L3 caches as a new level in the memory hierarchy to accelerate cache-intensive applications. In addition, a new instruction that performs indirectly addressed vector accumulation within a compute-capable LLC is added.

Since these combined improvements are expected to accelerate applications beyond the improvement of peak performance, application performance cannot be trivially estimated. We therefore carry out the first performance analysis of a next-generation vector supercomputer based on the VE30 processor. The main contributions of this paper are summarized as follows.

- This is the first work to evaluate the performance of a next-generation vector supercomputer equipped with VE30 processors. Using industry-standard benchmarks and several applications, we assess the real-world performance as well as the basic performance of VE30.
- This paper analyzes the performance gain obtained by each architectural improvement newly introduced in VE30 using microbenchmarks.
- This paper discusses performance tuning techniques to take advantages of the new architectural capabilities of VE30 to accelerate application performance.

The rest of this paper is organized as follows. Section 2 introduces the NEC SX-AT supercomputer and describes the basic architecture of the VE30 processor.

Section 3 extensively evaluates the performance of VE30 using standard benchmarks, microbenchmarks and real-world workloads. Section 4 discusses performance tuning techniques to fully exploit the potential of the VE30 processor. Section 5 concludes this paper.

2 Overview of SX-Aurora TSUBASA VE30

In this section, we first outline the architecture of the SX-AT supercomputer, and introduce the newly developed VE30 processor. We then describe the architectural enhancements of VE30 from its predecessor.

2.1 The SX-Aurora TSUBASA product family

The *SX-Aurora TSUBASA (SX-AT)* is the latest product family in the NEC SX vector supercomputers series. While SX-AT inherits the well-established and successful design philosophy of its predecessors, it also embraces the current *de facto* standard HPC software ecosystem. The first-generation SX-AT based on the Vector Engine 1.0 (VE10) processor was released in 2018 [11], which was followed by the second-generation SX-AT based on the Vector Engine 2.0 (VE20) processor released in 2020 [6]. The third-generation SX-AT based on the Vector Engine 3.0 (VE30) processor, which is evaluated in this paper, is currently under development and will be released in the near future.

SX-AT employs a heterogeneous architecture consisting of a *Vector Host (VH)* and a *Vector Engine (VE)*. The VH is an x86 server responsible for running the OS and performing tasks such as process and memory management and I/O. The VE is a vector processor implemented on a PCI Express (PCIe) card, and executes the application. The VH communicates with the VE over the PCIe link and controls the VE.

Although on the surface a VE resembles an accelerator such as a GPU, its execution model differs substantially from that of a conventional accelerator. Applications are fully executed on the VE, and system calls are forwarded to the VH and handled by proxy processes running on the VH. This design eliminates kernel launch overhead and reduces data transfer found in conventional accelerators. Furthermore, this design allows users to develop their applications using standard MPI and OpenMP-based programming models, and does not require any knowledge of a vendor-specific programming language or framework.

2.2 Basic Architecture of the VE30 Processor

Figure 1 illustrates an overview of a prototype VE30 processor, and Figure 2 depicts the memory hierarchy of a VE30 processor. The VE30 processor integrates 16 vector cores, a shared LLC and six HBM2E modules. Each vector core can perform up to 307.2 GFLOP/s (DP) or 614.4 GFLOP/s (SP), and thus a single socket performs 4.91 TFLOP/s (DP) or 9.83 TFLOP/s (SP) in total. The six HBM2E modules have 96 GB of capacity and provide an aggregate memory bandwidth of 2.45 TB/s to the cores. The shared LLC is 64 MB in size. The cores and LLC are interconnected through a 2-dimensional Network on Chip

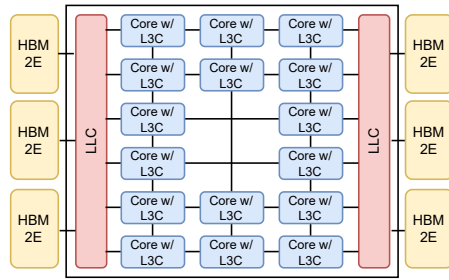


Fig. 1: Block diagram of the VE30 processor.

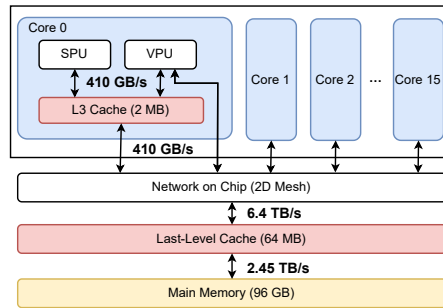


Fig. 2: Memory hierarchy of the VE30 processor.

(NoC). VE30 provides a *partitioning mode*, which splits the cores, LLC and HBM in the processor into two NUMA nodes. This increases the aggregate effective LLC bandwidth by alleviating congestion in the NoC, and benefits LLC-intensive applications.

A vector core in VE30 comprises a Scalar Processing Unit (SPU) and a Vector Processing Unit (VPU). The SPU fetches and decodes instructions, executes scalar instructions and dispatches vector instructions to the VPU. An SPU contains a 64 KB L1 instruction cache, a 64 KB L1 data cache, and a 512 KB unified L2 cache. A VPU contains 64 architectural vector registers that are renamed to 188 physical vector registers. A single vector register holds up to 256 double-precision floating point elements (*i.e.*, 2 KB). A VPU contains 32 vector pipelines, each of which has three Fused-Multiply Add (FMA) execution units. Thus, in total, a vector core can perform 96 FMA operations in a single cycle. The SPU and VPU share a 2 MB unified L3 cache.

2.3 Architectural Improvements from the VE20 Processor

VE30 features a significantly advanced memory subsystem compared to its predecessor. First, the introduction of a new level in the memory hierarchy, per-core private L3 caches, alleviates LLC contention and enables cache-intensive applications to achieve higher performance. Second, the LLC capacity and bandwidth are increased by 4× and 2.13×, respectively. Third, both the capacity and bandwidth of the HBM are also improved. The peak HBM bandwidth is increased by 1.60× from 1.53 TB/s to 2.45 TB/s, and the HBM capacity is doubled from 48 GB to 96 GB. These drastic improvements to the memory subsystem combined are expected to significantly accelerate both memory-intensive and cache-intensive applications.

In addition to the enhancements made to the memory subsystem, the core count is increased from 10 to 16 cores, which increases the peak single-socket performance from 3.07 TFLOP/s to 4.91 TFLOP/s. It should be noted that, despite the increase in the number of cores, the per-core cache and memory performance is either increased or maintained.

Furthermore, a number of improvements are made to the core. First, VE30 relaxes the alignment requirement for single-precision floating point vectors, and improves

the performance single-precision applications. Second, VE30 introduces a dedicated hardware mechanism for accelerating vector accumulation with indirect addressing. These improvements do not directly contribute to the peak FLOP/s rate, but are expected to benefit the performance of real-world applications.

3 Performance Evaluation

In this section, we first reveal the basic performance of VE30 using industry-standard benchmarks. We then use microbenchmarks to examine the performance gains delivered by architectural improvements introduced in VE30. Finally, we use workloads that represent practical applications to assess the real-world performance of VE30. Note that the performance measurements on VE30 are conducted using prototype software and hardware. Thus, the results may be subject to change on the final product.

3.1 Evaluation Environment

Table 1: Specifications of the evaluated processors.

	VE Type 20B	VE Type 30A	A64FX	Xeon Platinum 8368	A100 80 GB PCIe
Frequency [GHz]	1.6	1.6	2.2	2.4	1.412
Performance per Core [GFLOP/s]	307 (DP) 614 (SP)	307 (DP) 614 (SP)	70 (DP) 140 (SP)	83.2 (DP) ¹ 166 (SP)	181 (DP) w/ Tensor Core 90 (DP) w/o Tensor Core 181 (SP)
Number of Cores	8	16	48	38	108
Performance per Socket [TFLOP/s]	2.4 (DP) 4.9 (SP)	4.9 (DP) 9.8 (SP)	3.3 (DP) 6.7 (SP)	3.1 (DP) ¹ 6.3 (SP)	19.5 (DP) w/ Tensor Core 9.7 (DP) w/o Tensor Core 19.5 (SP)
LLC Bandwidth [TB/s]	3.0	6.4	3.6	3.2 ²	4.9 ²
LLC Capacity [MB]	16	64	32	54	40
Memory Bandwidth [TB/s]	1.53	2.45	1.024	0.204	1.935
Memory Capacity [GB]	48	96	32	256	80
Process Rule [nm]	16	7	7	10	7

Table 1 summarizes the specifications of the processors used in this evaluation. We compare VE30 to a variety of latest processors used in HPC spanning from a vector processor, GPU, many-core processor and general-purpose CPU: NEC Vector Engine Type 20B (an 8-core SKU of VE20) [6], NVIDIA A100 40 GB and 80 GB PCIe models [3], Fujitsu A64FX [21], and Intel Xeon Platinum 8368 (IceLake-SP) [16]. As shown in Table 1, the peak performance of A100 doubles when the Tensor Cores are included. We use the peak performance including the Tensor Cores when calculating the

¹ The peak performance is calculated based on the AVX-512 Turbo Frequency when all cores are active.

² The LLC bandwidth (L2 bandwidth on IceLake-SP) is measured using the Empirical Roofline Toolkit (<https://bitbucket.org/berkeleylab/cs-roofline-toolkit>) since the peak bandwidth is not disclosed by the manufacturers.

efficiency of HPL, and the peak performance excluding the Tensor Cores for the other benchmarks. This is because all benchmarks except HPL do not use the Tensor Cores.

Multi-node measurements for VE30 are carried out on a cluster composed of 16 VHs interconnected with a dual-rail InfiniBand HDR network. Each VH is equipped with eight Vector Engine Type 30A cards, an AMD EPYC 7713P processor and 512 GB of DDR4-3200 SDRAM.

3.2 Basic Benchmarks

We use four widely recognized benchmarks in HPC to evaluate the basic performance of VE30: the High Performance Linpack (HPL) [5] benchmark, STREAM benchmark, High Performance Conjugate Gradients (HPCG) [4] and Himeno benchmark [7].

HPL is a compute-intensive benchmark that solves a dense system of linear equations using LU decomposition with partial pivoting. The STREAM benchmark measures the effective memory bandwidth. HPCG is a memory-intensive benchmark that solves a sparse linear system using the conjugate gradient method and a geometric multigrid preconditioner. The Himeno benchmark is also memory-intensive, and solves the Poisson equation using the Jacobi method. Only the Himeno benchmark uses single-precision floating point numbers for computation and the rest use double-precision floating point numbers. Since HPL and HPCG executables optimized for the A64FX processor are unavailable to us, the HPL and HPCG performance of A64FX is calculated based on the Top500 result of an A64FX-based system (*Fugaku* [21]).

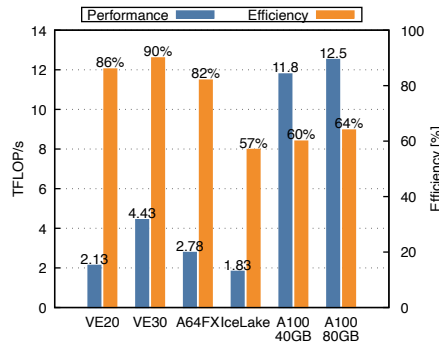


Fig. 3: HPL benchmark performance.

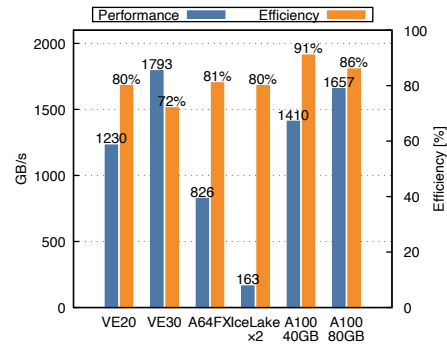


Fig. 4: Effective memory bandwidth.

Figure 3 compares the HPL performance of different processors. The NVIDIA A100 clearly stands out from the other processors. The A100 40 GB model achieves over 11.8 TFLOP/s in HPL performance, and the 80 GB model achieves a slightly higher performance of 12.5 TFLOP/s due to the increased problem size and higher TDP. The VE30 processor delivers 4.43 TFLOP/s and surpasses both A64FX and IceLake-SP. With respect to efficiency, VE30 is the highest with an efficiency of 90%, followed by A64FX and VE20. A100 shows relatively low efficiency as it cannot maintain the GPU boost clock due to power throttling.

Figure 4 compares the effective memory bandwidth of the different processors measured using STREAM. The effective memory bandwidth of VE30 exceeds 1.79 TB/s and is clearly the highest among the evaluated processors. Compared to its predecessor, VE20, the effective memory bandwidth of VE30 is 1.45× higher.

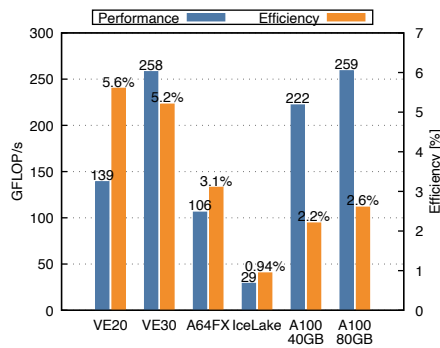


Fig. 5: HPCG benchmark performance.

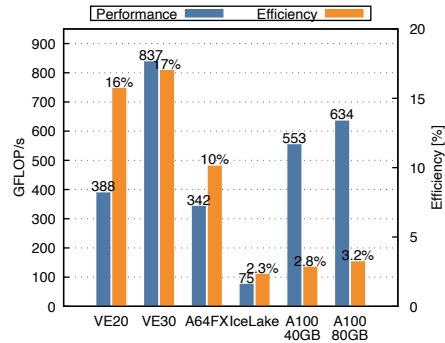


Fig. 6: Himeno benchmark performance (XL size).

Figure 5 shows the HPCG performance of the evaluated processors. VE30 attains 258 GFLOP/s and outperforms VE20, A64FX, IceLake-SP and the A100 40 GB model. It achieves almost identical performance as the A100 80 GB model. In terms of efficiency, VE30 achieves 5.2% of the peak performance, which is considerably higher than that of the other processors: 1.97× higher than the A100 80 GB model and 5.72× higher than IceLake-SP. Furthermore, VE30 achieves the highest energy efficiency among all processors. The energy efficiency of VE30 when executing HPCG reaches 1.034 GFLOP/s/W, while A100 40 GB and 80 GB models achieve 0.909 GFLOP/s/W and 0.999 GFLOP/s/W, respectively. These results highlight that VE30 successfully strikes the balance between memory performance and floating-point performance, whereas other processors heavily prioritize floating-point performance over memory performance.

Figure 6 shows the performance of the Himeno benchmark. VE30 is the best-performing one among all processors. It marks 837 GFLOP/s and surpasses the A100 40 GB and 80 GB models by a factor of 1.51× and 1.32×, respectively. Interestingly, the speedup exceeds the difference in memory bandwidth. For example, VE30 has 1.27× higher memory bandwidth than the A100 80 GB model, but its performance is 1.32× higher. The speedup over VE20 that achieves 388 GFLOP/s is 2.15×, which is again much larger than the 1.60× peak memory bandwidth improvement. This is likely because the alignment restriction for single-precision vectors is relaxed in VE30, and single-precision applications can be executed more efficiently.

Finally, we assess the multi-node scalability of HPL, HPCG and Himeno benchmarks. Figure 7 shows the multi-node performance of the two benchmarks as a function of the number of VEs. The results indicate that all three benchmarks scale almost linearly from 1 VE to 128 VEs with minor drop in efficiency. On 128 VEs, or 16 VHs, the HPL performance reaches 537 TFLOP/s with an efficiency of 85.5%. The HPCG benchmark

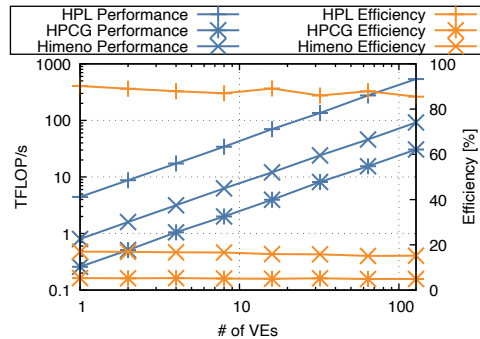


Fig. 7: Multi-node scaling performance of HPL, HPCG and Himeno benchmarks.

Table 2: Summary of the Tohoku University kernel collection.

Kernel	Domain	Bottleneck
Earthquake [1]	Seismology	Mem. B/W
Turbulent Flow [27]	Fluid dynamics	LLC B/W
Antenna [19]	Electronics	Mem. B/W
Land Mine [20]	Electronics	Mem. B/W
Turbine [27]	Fluid dynamics	Mem. latency
Plasma [10]	Geophysics	Mem. latency

achieves 30.6 TFLOP/s on 128 VEs with an efficiency of 4.9%. The Himeno benchmark achieves 919 TFLOP/s on 128 VEs with 15.2% efficiency.

3.3 Evaluation of Architectural Improvements

Bypassable L3 Cache VE30 incorporates per-core private L3 caches into the memory hierarchy. This design choice was made based on the observation that cache-intensive applications suffered from degraded LLC performance on previous generations of the VE. This is largely due to the congestion in the NoC and cache contention in the LLC. The introduction of private L3 caches is expected to improve the effective cache bandwidth by alleviating NoC congestion and LLC contention.

Furthermore, the L3 cache can be bypassed by software. Similar to non-temporal loads and stores in CPUs and GPUs [14], each load or store instruction can specify whether to bypass the L3 cache or not. Selectively caching data that exhibit high temporal locality is expected to reduce cache pollution and allow applications to efficiently utilize the limited cache capacity. From the programmer’s perspective, selective caching is enabled by inserting a compiler directive `#pragma _NEC on_adb(var)` in the source code, where `var` indicates the array to be L3-cached.

Note that the L3 cache bypassing is different from the LLC retention control [15] that was available in the previous VE generations. The LLC retention control allows applications to mark data as either temporal or non-temporal when issuing loads and stores. The LLC then prioritizes temporal data over non-temporal data when evicting cache lines. However, even if an access is marked as non-temporal, it is still cached in LLC. Thus, non-temporal data can still occupy a certain amount of the cache. The L3 cache bypassing, on the other hand, completely bypasses the L3 cache.

To assess the contribution of the L3 cache to application performance, we utilize the L3 cache bypassing feature and compare the performance of applications with and without enabling the L3 cache. Here, we use the *Tohoku University kernel collection* [11, 23], a set of computational kernels extracted from production applications developed by the users of the Cyberscience Center, Tohoku University. As summarized in Table 2, the

kernel collection comprises six kernels spanning a wide variety of scientific domains and performance characteristics.

Figure 8 presents the performance of each kernel with and without enabling the L3 cache. The results reveal that Turbulent Flow, Antenna, Turbine and Plasma clearly benefit from the L3 cache. Since the L3 cache saves LLC and memory bandwidths by serving portion of the memory requests, LLC-intensive and memory-intensive applications such as Turbulent Flow and Antenna are accelerated. Contrastingly, Earthquake and Land Mine do not benefit from the L3. These two kernels are memory-intensive and may either have poor data locality or a large working set size that does not fit in the L3 cache. The memory latency sensitive kernels, Turbine and Plasma, are also accelerated as the L3 cache reduces memory latency. Accessing the LLC incurs higher latency than the L3 cache since the LLC is physically farther away than the L3 cache, and requires communication over the potentially congested NoC.

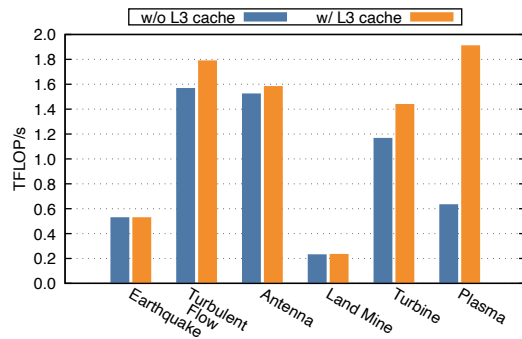


Fig. 8: Impact of L3 Cache on Tohoku University kernel collection performance.

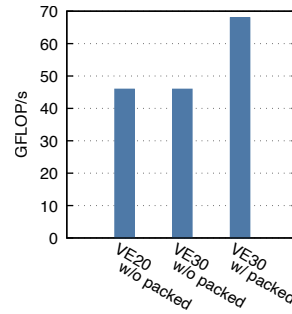


Fig. 9: Single-core performance of a single-precision 27-point stencil kernel.

Relaxed Alignment Restriction for Packed Instructions The *packed* instructions in SX-AT operate on vectors of 32-bit values, where each 64-bit element of a vector register holds a pair of 32-bit values. For example, a vector register can store 512 single-precision floating point numbers using the packed format. However, previous generations of the VE imposed an alignment restriction, requiring that the starting address of a packed vector is 8-byte aligned. Otherwise, the packed format cannot be used, and each element of a vector register holds only one 32-bit value instead of two. VE30 lifts this restriction and only requires 4-byte alignment for single-precision vectors.

To evaluate the speedup offered by the packed format, we measure the performance of a single-precision 27-point stencil kernel. Figure 9 presents the single-core performance of the 27-point stencil kernel on VE20 and on VE30 with and without using the packed format. Using the packed format on VE30 improves the performance by 1.48 \times compared to VE20 and VE30 without using the packed format.

Hardware Support for Indexed Vector Accumulation The VE30 processor introduces hardware support for vector accumulation with indirect addressing (*i.e.*, `axpyi` in Sparse BLAS). Such computation is fundamental in applications including finite element and particle methods. An example of an indexed vector accumulation is shown in Listing 1.1. In this example, array `y` is indirectly accessed using array `l[i]` as indices. This loop cannot be automatically vectorized by the compiler because loop-carried dependencies exist if some of the indices in `l` overlap.

Listing 1.1: Indexed vector accumulation.

```
for (int i = 0; i < n; i++)
    y[l[i]] = y[l[i]] + x[i];
```

Prior to VE30, programmers needed to manually examine whether `l[i]` may overlap, and either insert the `ivdep` or `list_vector` compiler directive to the loop. The `ivdep` directive is specified when there are no overlaps of indices, and simply vectorizes the loop. In the case where the indices do overlap, the `list_vector` directive must be specified. The `list_vector` directive instructs the compiler to generate a code that (1) computes the results using vector instructions ignoring loop-carried dependencies, (2) checks the overlaps of indices, and (3) corrects the results for overlapping indices using scalar instructions. However, the overhead incurred by the corrections increases as the number of overlapping indices in vector `l` increases.

VE30 adds specialized hardware for atomic accumulation in the LLC along with a new instruction, `vlfa`. The `vlfa` instruction sends the vector of indices (`l` in Listing 1.1) and the added vector (`x`) to the LLC, and then performs the accumulation in the LLC. The `vlfa` instruction should perform better than `list_vector` because scalar-based corrections are unneeded, and the latency of vector gather is eliminated. Programmer productivity is also improved since programmers no longer have to spend effort in identifying whether the indices might overlap or not. Note, however, that `vlfa` still slows down when the number of overlapping indices increases because contention may occur in the LLC.

To investigate the performance of the `vlfa` instruction, we use the indexed vector accumulation kernel shown in Listing 1.1. Here, we compare the following five variants: scalar-only on VE20 and VE30, `list_vector` on VE20 and VE30, and `vlfa` on VE30. We vary the number of overlapping indices to quantify the performance degradation caused by the overlap of indices. This is achieved by initializing the index vector `l` as the following:

$$l[i] = \begin{cases} 0 & \text{if } i \bmod 32 < k \\ i & \text{otherwise,} \end{cases} \quad (1)$$

where k is varied from 1 to 32.

Figure 10 shows the performance of indexed vector accumulation for each variant. Evidently, `vlfa` outperforms all other variants when the number of overlapping indices is small; it is 3.48× faster than `list_vector` and 4.72× faster than scalar-only when 4 out of 32 indices overlap. The performance of `vlfa` starts to decline with more than 8 overlapping indices, and falls below scalar-only with more than 20 identical indices. However, such large degree of address overlap is unlikely in real-world applications. This

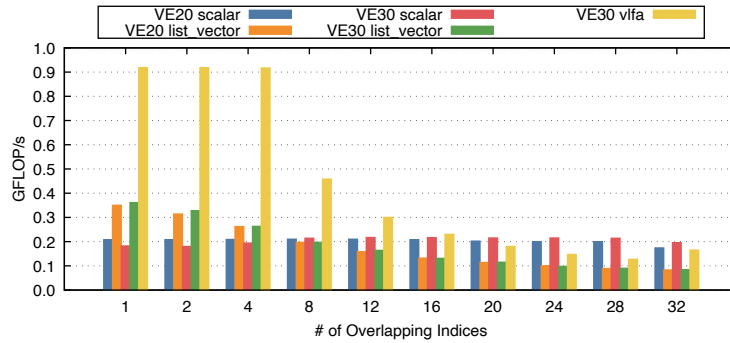


Fig. 10: Single-core performance of indexed vector accumulation.

Listing 1.2: A kernel loop involving indexed vector accumulation.

```

DO N = nstart, nend
  IF (flag3(N)==1) THEN
    COF(7, WI(N), WJ(N), WK(N))=COF(7, WI(N), WJ(N), WK(N))+W_TAUWC(N) * W_AREA_1(N)
    SOC(WI(N), WJ(N), WK(N))=SOC(WI(N), WJ(N), WK(N))+W_TAUWS(N) * W_AREA_1(N)
  ENDIF
ENDDO

```

indicates that programmers generally do not need to specify the `ivdep` or `list_vector` directives on VE30, hence the productivity is improved.

Listing 1.2 shows a kernel loop that appears in a real-world fluid dynamics application. Here, two 3-dimensional arrays `COF` and `SOC` are accumulated in a single loop. Prior to VE30, the VE compiler was unable to vectorize this kind of code. On VE30, the compiler can vectorize this code with the help of the `v1fa` instruction. As a result, this kernel takes 175.6s to run on VE30 without the `v1fa` instruction, but only takes 12.0s to run with the `v1fa` instruction, resulting in a 14.6× speedup.

3.4 Real-world Workloads

SPEChpc 2021 Benchmark Suite *SPEChpc* [24] is a benchmark suite developed by the Standard Performance Evaluation Corporation (SPEC), and comprises a set of carefully selected applications that represent a wide range of real-world HPC applications. The latest version of the SPEChpc benchmark suite, SPEChpc 2021, was released in October 2021. It supports multiple programming models and can run on both CPUs and GPUs. In this evaluation, we use MPI+OpenMP on VE20, VE30, A64FX and IceLake-SP, and MPI+OpenACC on A100.

We first use the *tiny* workload from the SPEChpc 2021 benchmark suite to compare the single-socket performance of the processors. The smallest tiny workload consists of nine benchmarks and requires approximately 60 GB of memory. We plot the speedups to a reference system (a 2-socket 12-core Intel Haswell system) reported by the SPEChpc benchmark script for each processor. If a processor needs more than one socket due

to the memory footprint requirement, the speedup is divided by the number of sockets to make a fair comparison. Since the compilers for VE30 are still under development as of writing this paper, we could not obtain the performance results for SOMA and Minisweep on VE30.

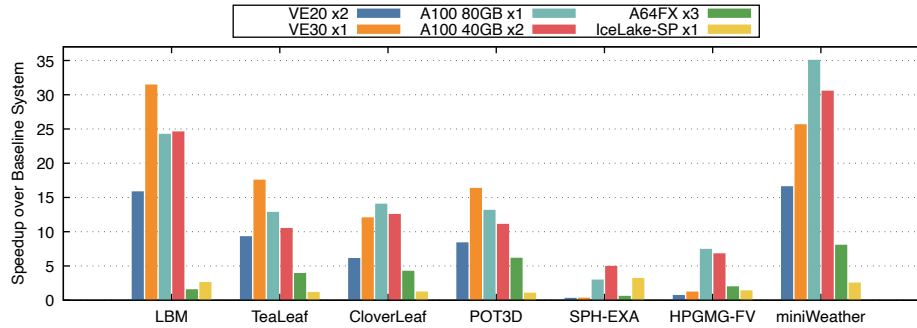


Fig. 11: SPEChpc 2021 tiny workload performance.

Figure 11 summarizes the SPEChpc tiny workload performance on the different processors. VE30 outperforms all other processors in LBM, TeaLeaf and POT3D. The speedups of these three benchmarks over the A100 80 GB model are 1.29 \times , 1.36 \times and 1.24 \times , respectively. The speedups of LBM and TeaLeaf exceed the difference in memory bandwidth, suggesting that the architectural enhancements such as the newly introduced L3 cache and increased LLC capacity and bandwidth, are contributing to the performance gain.

VE30 also clearly outperforms A64FX and IceLake-SP in CloverLeaf and miniWeather, but slightly underperforms the A100 40 GB and 80 GB models. This is because the time-consuming kernels in CloverLeaf require a large number of vector gather operations, and it appears that VE30 struggles at hiding the latency of vector gather operations compared to A100. The miniWeather benchmark contains a mix of memory-intensive and compute-intensive kernels. Although memory-intensive kernels are faster on VE30 than on A100, compute-intensive kernels are slower on VE30 and dominate the runtime.

SPH-EXA and HPGMG-FV perform poorly on VE30. SPH-EXA [2] is mainly bottlenecked by the construction of an octree-based spatial index and nearest neighbor queries over the index. Both of these functions inherently require recursive function calls and cannot be vectorized. To achieve better performance on vector processors, the nearest neighbor search needs to be changed to a vector-friendly algorithm.

HPGMG-FV suffers from short loop length. The HPGMG-FV tiny workload decomposes a 512^3 cubic domain into 32^3 cubic boxes and distributes the boxes to MPI ranks. The most time-consuming Gauss-Seidel Red-Black smoother kernel sweeps over a box with a triple-nested loop each corresponding to a spatial dimension. As a result, each loop runs for 32 times, but this is too short compared to the vector length of a VE, which is 256 double-precision elements. A potential optimization is collapse the nested loops

and increase the loop length. Another possible optimization is to offload the coarse grid levels to the VH and process fine grid levels on the VE.

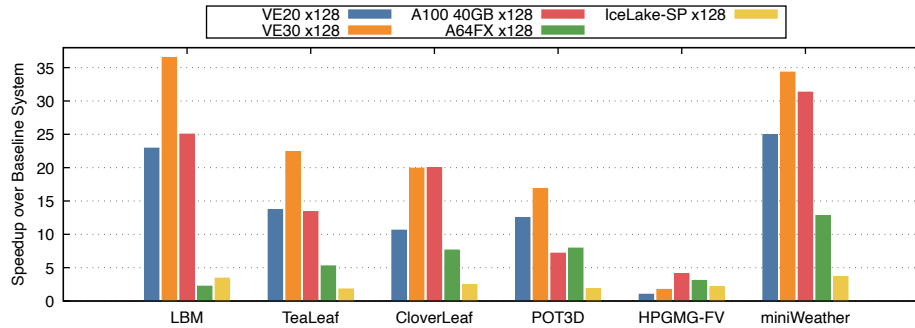


Fig. 12: SPEChpc 2021 medium workload performance.

To evaluate the multi-node scalability, we also compare the performance of the SPEChpc *medium* workload. The medium workload consists of six benchmarks and requires approximately 4 TB of memory. Here, we execute the workload using 128 sockets on all processors. Results for the A100 80 GB model are unavailable since we do not have access to a large-scale deployment of the A100 80 GB model. Figure 12 summarizes the medium workload performance. Here, VE30 is the fastest in four out of the six benchmarks, which are LBM, TeaLeaf, POT3D and miniWeather. Compared to the tiny workload, the speedup of VE30 over A100 is larger in the medium workload. For example, POT3D is 2.34 \times faster on VE30 compared to A100 in the medium workload, but it is only 1.47 \times faster in the tiny workload. This suggests that VE30 provides better multi-node scalability than A100.

Tohoku University Kernel Collection As described in Section 3.3, the Tohoku University kernel collection represents real-world applications developed by the users of the Cyberscience Center at Tohoku University. Figure 13 shows the performance of the Tohoku University kernels on VE20 and VE30. Evidently, VE30 consistently outperforms VE20 with all kernels. The speedup is especially significant for Turbulent Flow, Turbine and Plasma, all of which perform more than 2.3 \times faster on VE30 than on VE20. Given that Turbulent Flow is bound by LLC bandwidth on VE20, we believe the performance gain is obtained from the 2.13 \times LLC bandwidth increase and the newly added L3 cache. Turbine and Plasma benefit from the reduction in memory latency thanks to the L3 cache as discussed in Section 3.3.

Rainfall-Runoff-Inundation Model The Rainfall-Runoff-Inundation (RRI) Model [22, 26] is a 2-dimensional numerical model that is widely adopted in Japan to conduct flood forecasts. The governing equations are solved using the fifth-order Runge-Kutta method with adaptive time step control. From the computational point of view, the major kernels in the RRI model are memory-intensive, thereby suited for execution on VEs.

In this evaluation, we use an implementation of the RRI model optimized for SX-AT, and measure the runtime required for conducting a 2-hour flood prediction in the entire *Tohoku* region of Japan. Figure 14 shows the runtime of the flood prediction on VE20 and VE30. VE30 achieves 1.32 \times higher performance than VE20. The speedup of the parallel regions is 1.60 \times . Considering that the peak memory bandwidth is increased by 1.60 \times from VE20 to VE30 and the RRI model is memory-intensive, the observed speedup matches the expectation.

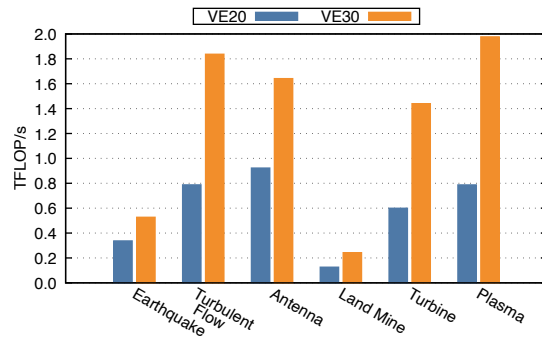


Fig. 13: Tohoku University kernel collection performance.

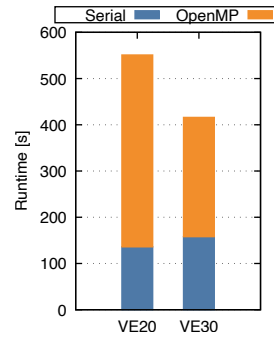


Fig. 14: Runtime of a 2-hour flood prediction using the RRI model.

4 Performance Tuning for VE30

Basic optimization techniques for VE include facilitating vectorization by factoring out unvectorizable code from loops, increasing the vector length using various loop transformations, and offloading unvectorizable computation to the VH. In addition to these optimization techniques, further performance can be exploited by utilizing the architectural features introduced in VE30. In this section, we present such tuning techniques and quantify their performance impact.

4.1 Selective L3 Caching

On VE30, programmers can take advantage of the bypassable L3 cache to selectively cache frequently reused data. To demonstrate the effect of selective L3 caching, we use the Himeno benchmark as an example. Listing 1.3 shows the time-consuming Jacobi kernel in the Himeno benchmark. Arrays *a*, *b*, *c*, *wrk1* and *bnd* are accessed in a consecutive manner and not reused. On the other hand, array *p* is accessed in a stencil-like manner. Although ideally 18 out of 19 accesses to *p* should hit in cache, the accesses to the other arrays pollute the cache and degrade the cache hit ratio of *p*. This cache pollution can be mitigated by caching *p* only and bypassing the cache when accessing *a*, *b*, *c*, *wrk1* and *bnd*.

Listing 1.3: Jacobi method kernel in the Himeno benchmark.

```

for(i=1 ; i<imax-1 ; ++i)
for(j=1 ; j<jmax-1 ; ++j)
for(k=1 ; k<kmax-1 ; ++k){
s0 = a[0][i][j][k] * p[i+1][j ][k ] + a[1][i][j][k] * p[i ][j+1][k ]
+ a[2][i][j][k] * p[i ][j ][k+1]
+ b[0][i][j][k] * ( p[i+1][j+1][k ] - p[i+1][j-1][k ]
- p[i-1][j+1][k ] + p[i-1][j-1][k ] )
+ b[1][i][j][k] * ( p[i ][j+1][k+1] - p[i ][j-1][k+1]
- p[i ][j+1][k-1] + p[i ][j-1][k-1] )
+ b[2][i][j][k] * ( p[i+1][j ][k+1] - p[i-1][j ][k+1]
- p[i+1][j ][k-1] + p[i-1][j ][k-1] )
+ c[0][i][j][k] * p[i-1][j ][k ] + c[1][i][j][k] * p[i ][j-1][k ]
+ c[2][i][j][k] * p[i ][j ][k-1] + wrk1[i][j][k];
ss = ( s0 * a[3][i][j][k] - p[i][j][k] ) * bnd[i][j][k];
wgosa += ss*ss;
wrk2[i][j][k] = p[i][j][k] + omega * ss;
// Copy wrk2 to wrk and sum wgosa across all ranks
}

```

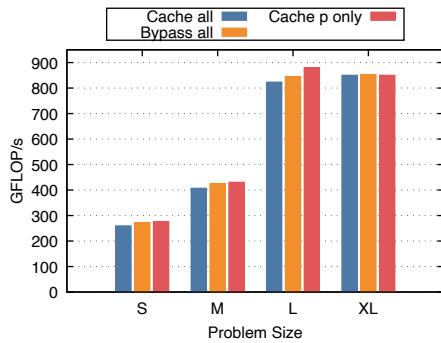
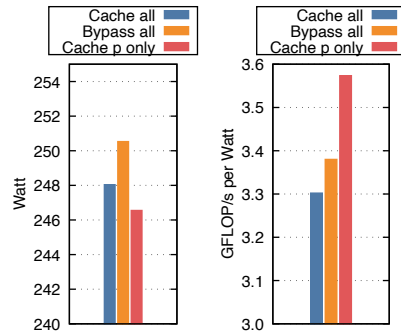


Fig. 15: Performance of Himeno benchmark with different problem sizes and L3 caching policies.



(a) Power Consumption- (b) Power Efficiency

Fig. 16: Power efficiency of Himeno benchmark (L size).

Figure 15 compares the performance of the Himeno benchmark under three different caching policies: (1) cache all arrays in the L3 cache, (2) always bypass the L3 cache, and (3) only cache p in the L3 cache. We also compare four different problem sizes: S ($2^6 \times 2^6 \times 2^7$), M ($2^7 \times 2^7 \times 2^8$), L ($2^8 \times 2^8 \times 2^9$), and XL ($2^9 \times 2^9 \times 2^{10}$). The results indicate that caching all arrays does not show any notable improvement over bypassing all arrays. This suggests that the L3 cache is polluted by non-temporal data and thus the cache hit ratio of p is low. Selectively caching p improves 6.5%, 5.7% and 6.9% over caching all arrays for problem sizes S, M and L, respectively. This indicates that selective caching alleviates cache pollution. Contrastingly, no performance improvement is observed for the XL problem size. This is because p does not fit in the L3 cache in the XL size.

To investigate if selective caching has an impact on power consumption and power efficiency, we use the NEC Monitoring & Maintenance Manager (MMM)⁴ tool and measure the power consumption of the VE30 PCIe card while running the Himeno benchmark. Figure 16 compares the power consumption and efficiency of the VE30 card under different caching policies. The results indicate that selectively caching p reduces the power consumption by 0.6% compared to caching all arrays because the number of memory accesses is reduced. Combined with the performance improvement, selective caching improves the power efficiency by 8.2%, resulting in a power efficiency of 3.57 GFLOP/s/W. Compared to VE20 that achieves 2.21 GFLOP/s/W and the A100 40 GB model that achieves 2.14 GFLOP/s/W [12], VE30 achieves 1.61 \times and 1.66 \times higher power efficiency, respectively.

Furthermore, we apply selective L3 caching to the Land Mine kernel to study if selective caching is beneficial for real-world applications. Figure 17 shows the performance, power consumption and power efficiency of the Land Mine kernel under different L3 caching policies. Bypassing the L3 cache yields the lowest performance of 299 GFLOP/s. Enabling the cache slightly improves the performance to 312 GFLOP/s, and selective caching further improves the performance to 339 GFLOP/s. In terms of power consumption, caching all arrays and selective caching both consume slightly more power than bypassing the cache. This is because the increase in cache power outweighs the reduction in memory power. However, the performance gain of selective caching is large enough that its power efficiency is the highest.

4.2 Partitioning Mode

As mentioned in Section 2.2, the partitioning mode increases the effective LLC bandwidth by relieving the congestion in the NoC that interconnects the cores and the LLC. Therefore, enabling the partitioning mode may accelerate cache-intensive applications. Although the partitioning mode has been available in the previous generations of VEs, its benefits are expected to be larger on VE30 since NoC congestion becomes heavier due to the increased number of cores.

To assess the effect of the partitioning mode on VE30, we measure the performance of the Himeno benchmark with and without the partitioning mode. The results are shown

⁴ https://sxaurooratsubasa.sakura.ne.jp/documents/guide/pdfs/InstallationGuide_E.pdf

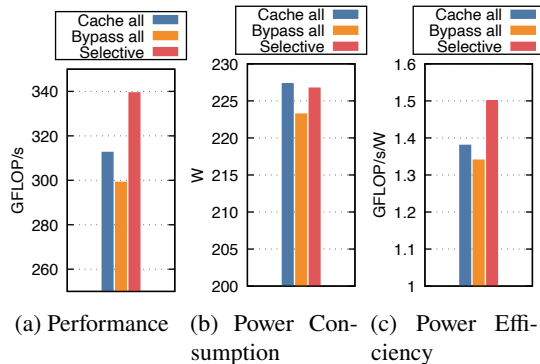


Fig. 17: Performance and power efficiency of the Land Mine kernel under different L3 caching policies.

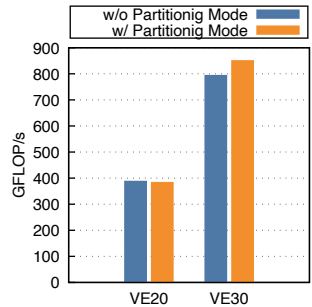


Fig. 18: Impact of the partitioning mode to Himeno benchmark performance (XL size).

in Figure 18. As expected, the partitioning mode does not have a significant impact on VE20 since the NoC is not congested. Contrastingly, the performance is increased by 7.1% by enabling the partitioning mode on VE30. This suggests that the NoC congestion is alleviated by the partitioning mode. Thus, the use of partitioning mode should be considered when running cache-intensive applications on VE30.

5 Conclusions

In this paper, we carried out an extensive performance evaluation of a next-generation SX-AT supercomputer equipped with the brand-new VE30 processor. VE30 attains massive performance in memory-intensive standard benchmarks such as the Himeno benchmark and outperforms other processors. The speedup of VE30 over the other processors exceeds the difference in the peak compute and memory performance, indicating the benefits of the novel architectural enhancements introduced in VE30. VE30 also outperforms other processors in many real-world applications such as SPEChpc. Finally, we presented performance tuning techniques to fully exploit the potential of VE30.

These evaluation results clearly demonstrate that VE30 can achieve high sustained performance comparable to latest GPUs and CPUs, while allowing programmers to use conventional programming models, *i.e.*, MPI+OpenMP. This proves the next-generation SX-AT to be an attractive choice for users seeking real-world application performance.

Acknowledgments

This work was partially supported by JSPS KAKENHI Grant Numbers JP20H00593, JP20K19808, JP21H03449 and JP22K19764. Part of the experiments were carried out using *AOBA-A* and *AOBA-C* at the Cyberscience Center, Tohoku University, *Flow* at the Information Technology Center, Nagoya University, and *SQUID* at the Cybermedia Center, Osaka University.

References

1. Ariyoshi, K., Matsuzawa, T., Hasegawa, A.: The key frictional parameters controlling spatial variations in the speed of postseismic-slip propagation on a subduction plate boundary. *Earth and Planetary Science Letters* **256**(1-2), 136–146 (2007)
2. Cavelan, A., Cabezón, R.M., Grabarczyk, M., Ciorba, F.M.: A Smoothed Particle Hydrodynamics Mini-App for Exascale. Platform for Advanced Scientific Computing Conference (PASC'20) pp. 1–11 (Jun 2020)
3. Choquette, J., Gandhi, W., Giroux, O., Stam, N., Krashinsky, R.: NVIDIA A100 Tensor Core GPU: Performance and Innovation. *IEEE Micro* **41**(2), 29–35 (2021)
4. Dongarra, J., Heroux, M.A., Luszczek, P.: High-performance conjugate-gradient benchmark: A new metric for ranking high-performance computing systems. *International Journal of High Performance Computing Applications* **30**(1), 3–10 (2016)
5. Dongarra, J.J., Luszczek, P., Petite, A.: The LINPACK benchmark: Past, present and future. *Concurrency and Computation: Practice and Experience* **15**(9), 803–820 (2003)
6. Egawa, R., Fujimoto, S., Yamashita, T., Sasaki, D., Isobe, Y., Shimomura, Y., Takizawa, H.: Exploiting the Potentials of the Second Generation SX-Aurora TSUBASA. In: Performance Modeling, Benchmarking and Simulation of High Performance Computer Systems (PMBS 2020). vol. 2, pp. 39–49 (2020)
7. Himeno, R.: Himeno benchmark, <https://i.riken.jp/en/supercom/documents/himenobmt/>
8. Hsu, K.C., Tseng, H.W.: Accelerating applications using edge tensor processing units. In: International Conference for High Performance Computing, Networking, Storage and Analysis (SC21). pp. 1–14 (Nov 2021)
9. Jouppi, N.P., Hyun Yoon, D., Ashcraft, M., Gottscho, M., Jablin, T.B., Kurian, G., Laudon, J., Li, S., Ma, P., Ma, X., Norrie, T., Patil, N., Prasad, S., Young, C., Zhou, Z., Patterson, D.: Ten Lessons From Three Generations Shaped Google's TPUv4i. In: 48th Annual International Symposium on Computer Architecture (ISCA). pp. 1–14 (Jun 2021)
10. Katoh, Y., Ono, T., Iizima, M.: Numerical simulation of resonant scattering of energetic electrons in the outer radiation belt. *Earth, Planets and Space* **57**(2), 117–124 (2005)
11. Komatsu, K., Momose, S., Isobe, Y., Watanabe, O., Musa, A., Yokokawa, M., Aoyama, T., Sato, M., Kobayashi, H.: Performance Evaluation of a Vector Supercomputer SX-Aurora TSUBASA. In: International Conference for High Performance Computing, Networking, Storage and Analysis (SC18). pp. 685–696 (Nov 2018)
12. Komatsu, K., Onodera, A., Focht, E., Fujimoto, S., Isobe, Y., Momose, S., Sato, M., Kobayashi, H.: Performance and Power Analysis of a Vector Computing System. *Supercomputing Frontiers and Innovations* **8**(2), 75–94 (2021)
13. Louw, T., Mcintosh-Smith, S.: Using the Graphcore IPU for Traditional HPC Applications. In: 3rd Workshop on Accelerated Machine Learning (AccML) (Jan 2021)
14. Mittal, S.: A survey of cache bypassing techniques. *Journal of Low Power Electronics and Applications* **6**(2) (2016)
15. Onodera, A., Komatsu, K., Fujimoto, S., Isobe, Y., Sato, M., Kobayashi, H.: Optimization of the Himeno Benchmark for SX-Aurora TSUBASA. *Lecture Notes in Computer Science (including subseries Lecture Notes in Artificial Intelligence and Lecture Notes in Bioinformatics)* **12614 LNCS**, 127–143 (2021)
16. Papazian, I.E.: New 3rd Gen Intel® Xeon® Scalable Processor. In: Hot Chips Symposium (2020)
17. RISC-V Foundation: RISC-V "V" Vector Extension. Tech. rep. (2021), <https://github.com/riscv/riscv-v-spec/releases/tag/v1.0>

18. Rocki, K., Essendelft, D.V., Sharapov, I., Schreiber, R., Morrison, M., Kibardin, V., Portnoy, A., Dietiker, J.F., Syamlal, M., James, M.: Fast stencil-code computation on a wafer-scale processor. In: International Conference for High Performance Computing, Networking, Storage and Analysis (SC20) (Nov 2020)
19. Sato, H., Takagi, Y., Sawaya, K.: High gain antipodal fermi antenna with low cross polarization. *IEICE Transactions on Communications* **E94-B**(8), 2292–2297 (2011)
20. Sato, M., Kobayashi, T., Zeng, Z., Fang, G., Feng, X.: High resolution GPR system for landmine detection. In: Proceedings of International Conference Requirements and Technologies for the Detection, Removal and Neutralization of Landmine and UXO. pp. 548–553 (2003)
21. Sato, M., Ishikawa, Y., Tomita, H., Kodama, Y., Odajima, T., Tsuji, M., Yashiro, H., Aoki, M., Shida, N., Miyoshi, I., Hirai, K., Furuya, A., Asato, A., Morita, K., Shimizu, T.: Co-Design for A64FX Manycore Processor and "Fugaku". In: International Conference for High Performance Computing, Networking, Storage and Analysis (SC20). pp. 1–15 (Nov 2020)
22. Shimomura, Y., Musa, A., Sato, Y., Konja, A., Cui, G., Aoyagi, R., Takahashi, K., Takizawa, H.: A Real-time Flood Inundation Prediction on SX-Aurora TSUBASA. In: 29th International Conference on High Performance Computing, Data, and Analytics (HiPC) (2022)
23. Soga, T., Musa, A., Shimomura, Y., Egawa, R., Itakura, K., Takizawa, H., Okabe, K., Kobayashi, H.: Performance evaluation of NEC SX-9 using real science and engineering applications. In: International Conference on High Performance Computing Networking, Storage and Analysis (SC'09). pp. 1–12 (Nov 2009)
24. Standard Performance Evaluation Corporation: SPEC_{hpc} 2021 (2021), <https://www.spec.org/hpc2021/>
25. Stephens, N., Biles, S., Boettcher, M., Eapen, J., Eyole, M., Gabrielli, G., Horsnell, M., Magklis, G., Martinez, A., Premillieu, N., Reid, A., Rico, A., Walker, P.: The ARM Scalable Vector Extension. *IEEE Micro* **37**(2), 26–39 (2017)
26. The International Centre for Water Hazard and Risk Management: Rainfall-Runoff-Inundation (RRI) model, <https://www.pwri.go.jp/icharm/research/rri/index.html>
27. Tsukahara, T., Iwamoto, K., Kawamura, H.: Evolution of Material Line in Turbulent Channel Flow. In: the 5th International Symposium on Turbulence and Shear Flow Phenomena. pp. 549–554 (2007)